NeuroImage 44 (2009) 136–144

Contents lists available at ScienceDirect

NeuroImage

journal homepage: www.elsevier.com/locate/ynimg

A framework to analyze partial volume effect on gray matter mean diffusivity measurements

Bang-Bon Koo [a], Ning Hua [b], Chi-Hoon Choi [a,c], Itamar Ronen [d,e], Jong-Min Lee [a], Dae-Shik Kim [d,e,*]

[a] Department of Biomedical Engineering, Hanyang University, Seoul, South Korea
[b] Department of Biophysics, Boston University School of Medicine, Boston, MA 02118, USA
[c] Department of Radiology, National Medical Center, Seoul, South Korea
[d] Center for Biomedical Imaging (CBI), Boston University Medical Center, Boston, MA 02118, USA
[e] Department of Anatomy and Neurobiology, Boston University School of Medicine, 715 Albany Street L-1004, Boston, MA 02118, USA

ARTICLE INFO

Article history:
Received 20 May 2008
Revised 20 July 2008
Accepted 29 July 2008
Available online 15 August 2008

ABSTRACT

Analyzing gray matter diffusion properties can be challenging due to possible measurement biases originating from averaging of gray matter (GM) and cerebrospinal fluid (CSF) signals. Therefore, a better characterization of CSF contamination effects in different cortical regions is required in order to disentangle actual changes in microstructure of GM itself from changes due to other effects such as macroscopic morphological changes. We propose a localized analysis framework for the CSF contamination effect on GM mean diffusivity measurement and applied this framework to measurements on 15 subjects. Our proposed modeling framework was compared to fluid-attenuated inversion recovery (FLAIR) DTI technique from the same subjects. The results of our studies suggest that GM mean diffusivity value was significantly biased by the CSF contamination effect, and that the amount of contamination strongly depended on the local morphology of the peripheral brain. Expected biases had their maxima in the motor and the somatosensory association cortex, and their minima in mid and inferior temporal areas of the brain where the cortical thicknesses are particularly pronounced. We conclude from our studies that regional differences in tissue compounding ratio must be taken into account when assessing localized GF diffusivity differences.

Introduction

Understanding the microstructural characteristics of the human brain in relation to neurophysiological and/or neuropathological phenomena is an important issue in clinical and basic neurosciences. Here, diffusion tensor imaging (DTI) based techniques have proven to be a potentially important technique for microstructural analysis of the brain (Basser, 1995; Beaulieu, 2002; Moseley, 2002). In many of the DTI applications, a scalar DTI index such as mean diffusivity has been used to provide anatomical contrast in a variety of clinical etiologies such as aging, Alzheimer's disease, and brain tumors (Horsfield and Jones, 2002; Kubicki et al., 2002). However, unlike the successful utilization of mean diffusivities for characterizing white matter (WM) and deep gray matter (GM) structures (Camara et al., 2007; Kubicki et al., 2002; Neil et al., 2002), its likewise applicability for cortical gray matter has been questioned (Benedetti et al., 2006; Helenius et al., 2002).

On the other hand, several lines of recent studies raise both the possibility of cortical gray matter mean diffusivity measurements for detecting specific diseases characteristics. For example, cortical GM mean diffusivity measurements were successfully applied to detect deterioration of primary progressive multiple sclerosis patients (Rovaris et al., 2002, 2006). Also, significant elevation of GM mean diffusivity was reported on mild cognitive impairment patients (Ray et al., 2006), congenital central hypoventilation syndrome (Kumar et al., 2006) and Creutzfeldt–Jakob disease (Liu et al., 2006). However, the veracity of these results have to remain partially elusive as the highly convoluted, thin-layered structure of the peripheral GM (Zilles et al., 1988) coupled with the limited acquisition resolution (2–5 mm) for conventional DTI will produce significant amount of partial voluming biases. For example, averaging GM and cerebrospinal fluid (CSF) containing voxels with each other may introduce critical measurement biases such as overestimated mean diffusivity (Alexander et al., 2001), and will depend on the volume of the fluid-filled spaces (Le Bihan, 1995; Niendorf et al., 1996). Observed GM mean diffusivity differences can therefore potentially be due to CSF contamination effect as well due to genuine differences in diffusivity from the underlying structures. Therefore, a better characterization of CSF contamination effects in different cortical regions will be critical to distinguish actual changes in microstructure of GM itself from changes due to other effects such as macroscopic morphological changes.

Although an estimation of the CSF contamination effect was introduced through the use of partial volume simulation (Le Bihan, 1995; Niendorf et al., 1996), currently there are no established means of interpreting the local GM diffusion measurements in relation to

* Corresponding author. Department of Anatomy and Neurobiology, Boston University School of Medicine, 715 Albany Street L-1004, Boston, MA 02118, USA. Fax: +1 617 414 2362.
E-mail address: dskim@bu.edu (D.-S. Kim).

1053-8119/$ – see front matter © 2008 Elsevier Inc. All rights reserved.
doi:10.1016/j.neuroimage.2008.07.064

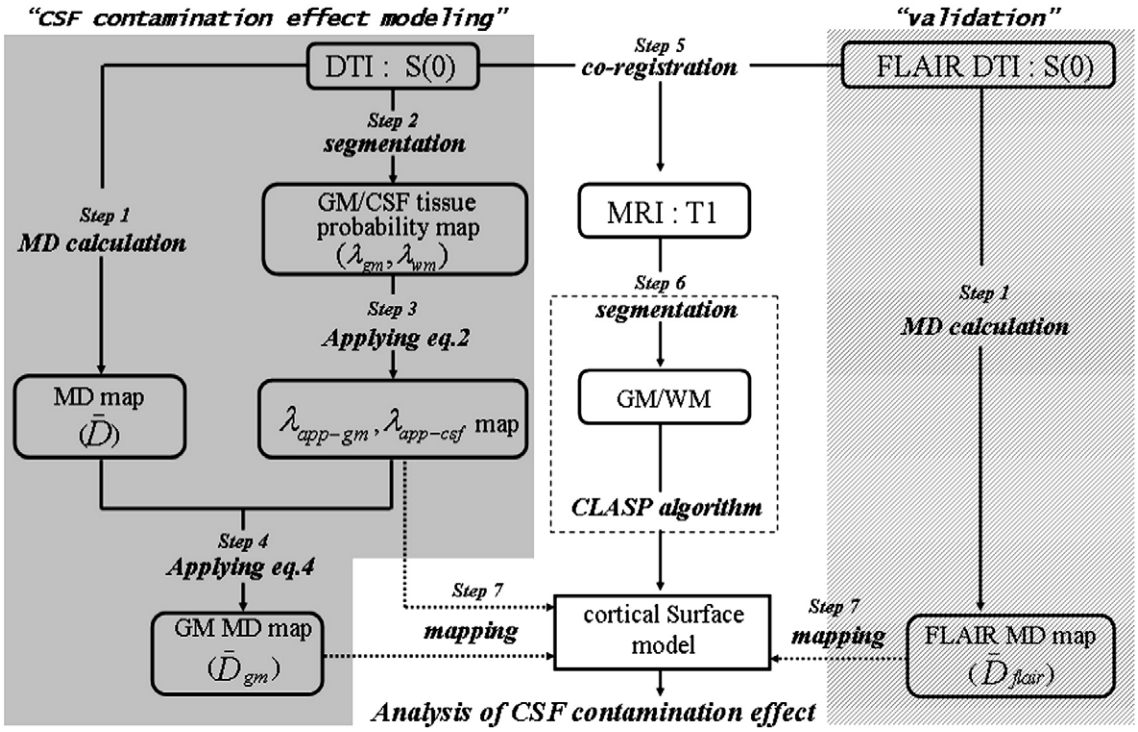

Fig. 1. Pipeline of CSF contamination effect modeling framework. The order of processing was numbered in the figure (steps 1–7). Here, T1 denotes high resolution anatomical volume; DTI $S(0)$ is non-diffusion weighted ($b=0$) volume; $\lambda_{app\text{-}gm}$ and $\lambda_{app\text{-}csf}$ denote apparent signal fraction weightings for GM and CSF compartment; FLAIR DTI $S(0)$ is non-diffusion weighted volume of FLAIR DTI; MD map denotes mean diffusivity map ($\bar{D}$); GM MD map denotes mean diffusivity map after correction ($\bar{D}_{gm}$); FLAIR DTI MD map denotes $\bar{D}_{flair}$.

potential biases. For a detailed assessment of the local CSF contamination effect, estimation of the local peripheral brain structure is required. An important step for estimating local brain structure is tissue segmentation to classify each image voxel to a particular tissue class. However, limited resolution of DTI increases the probability of misclassification. Likewise, a simple thresholding resulting in binary tissue class will be not appropriate for estimating the CSF contamination effect on DTI measurement. Thus, relatively fine resolution DTI data with proper modeling framework for partial volume averaging is needed.

Alternatively, CSF contamination may also be corrected using more specialized acquisition protocols, such as the fluid-attenuated inversion recovery (FLAIR) DTI technique (Falconer and Narayana, 1997; Kwong et al., 1991). However, while FLAIR DTI can suppress extracortical CSF signals, it is more time consuming than non fluid-attenuated sequences, hampering its use where time-efficiency is critical, such as in pediatric imaging.

In order to extend the effect of CSF contamination to group data, optimal registration and visualization are also important. Many of the current cortical surface modeling methods are capable of defining the boundaries between different brain tissues with subvoxel accuracy (Dale et al., 1999; Fischl et al., 1999; Kim et al., 2005; Lee et al., 2006), and the overall characteristics of cortex can be efficiently confirmed from 3 dimensional representation of cortical surface. The efficiency of the surface-based approach for matching homologous brain regions between subjects (Lyttelton et al., 2007) can help to improve the definition of group-specific patterns in each cortical region. Therefore, cortical surface modeling methods have been applied to increase the accuracy of functional data (Jo et al., 2007; Park et al., 2006) and for the structural analysis of the cortex (Benedetti et al., 2006). Here, cortical surface modeling method was applied for assessing group-specific regional CSF contamination patterns in relation to macroscopic morphology of peripheral brain.

The purpose of this study was firstly to develop a regional modeling technique for the CSF contamination effect. Here, GM mean diffusivity without CSF contamination effect was estimated from the proposed method, and the result was compared to FLAIR DTI dataset for testing the efficiency. Second goal of this study was to interpret the relevance of CSF contamination in measuring GM mean diffusivity in localized areas in order to better assess group characteristics. We hypothesized that the CSF contamination effect might have region specific patterns due to local morphological differences. Therefore, regional patterns were assessed based on the proposed method. Additionally, both cortical thickness and local curvature of GM were used to interpret the local CSF contamination effect in terms of the morphological characteristics of GM.

Methods

Data acquisition

MRI scans were performed on 15 right-handed, healthy, male subjects (age range: 22–34 years) using a 3 T Philips Intera system with institutional approvals. An MPRAGE sequence was applied to acquire high resolution anatomical images (T1), and the Single Shot-EPI was used in DTI. FLAIR DTI was obtained using same Single Shot-EPI from same group for validation purposes. For conventional DTI, the following parameters were used: TR=7–8 s (depending on the slice number), TE=90 ms, $b=1000$ s/mm^2, number of gradient directions=15, slice thickness=2 mm, FOV=240 mm, matrix size=128 after zero filling, AVG=3, scan time=2–3 min. For the FLAIR DTI experiments, the

Table 1
Symbols and meanings

Symbols	Meanings
$S(0)$	Non diffusion weighted volume.
D	Observed mean diffusivity value with CSF contamination effect
D_{gm}	Estimated mean diffusivity value of GM
D_{csf}	Estimated mean diffusivity value of CSF
D_{flair}	Estimated mean diffusivity value of GM from FLAIR DTI
λ_{csf}, λ_{gm}	Estimated volume ratio of the CSF and GM tissue
$\lambda_{app\text{-}gm}$, $\lambda_{app\text{-}csf}$	Estimated apparent volume fraction of the CSF and GM tissue

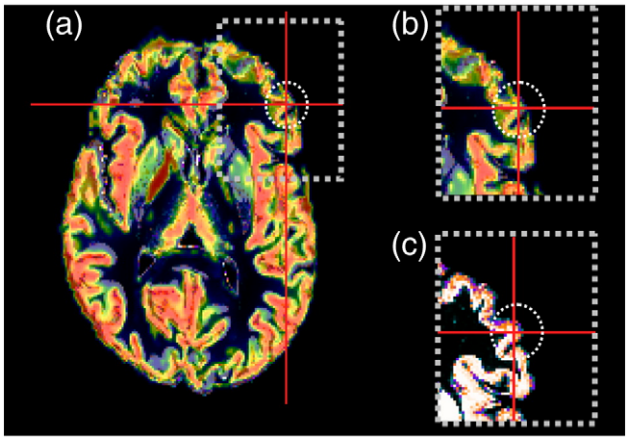

Fig. 2. Concept of local probabilistic similarity index measurement. Overlap figure between T1 GM tissue compartment and DTI GM compartment is in (a). A Part of GM compartment and T1 GM compartment are plotted in (b) and (c). Local PSI index is calculated in dotted circle.

parameters used were identical to the DTI except that the TR = 10 s and the AVG = 5. A 180 degree inversion recovery pulse was added before the conventional DTI sequence with a delay of 2200 ms. To reduce the inflow artifact, a 50% wider inversion pulse was used, and the slices were divided into 2 packages, which increased the scan time to 6–7 min. Here, all T1-weighted and DTI data were scanned in same session with same FOV for providing more relevant coregistration process.

Description of the CSF contamination model

Diffusion coefficient measurement depends on the composition of tissue compartments in each voxel. Thus, signal intensity measured for a voxel can be represented as the weighted sum of signals from all independent components by assuming no spin exchange between different tissue compartments. Because the mean diffusivity value of peripheral WM has been reported to have a similar range to GM, a two-tissue compartment model was applied and extended to the surface-based regional modeling in this study.

$$S(b) = S(0)\cdot[\lambda_{app-gm}\cdot\exp(-bD_{gm}) + \lambda_{app-csf}\cdot\exp(-bD_{csf})], \quad (1)$$

where $S(b)$ and $S(0)$ are the signal intensities of diffusion weighted and non-weighted signals, and $\lambda_{app\text{-}gm}$ and $\lambda_{app\text{-}csf}$ are the apparent signal fraction weightings of the GM and CSF compartment.

From Latour and Warach (2002), apparent signal fraction weighting can be expressed as:

$$\lambda_{app-i} = \frac{\lambda_i \cdot S_i(0)}{\sum_j \lambda_j \cdot S_j(0)}. \quad (2)$$

Here, λ_i is the estimated volume probability of existence for each tissue compartment (λ_{gm} for GM compartment; λ_{csf} for CSF compartment) in a single voxel. Index j is the total number of tissue compartments. $S_i(0)$, regarded as solely weighted by relaxation, is the signal intensity in the absence of diffusion gradients in spin-echo sequence and is defined as follows:

$$S_i(0) = \rho_i \cdot \exp\left[\frac{-TE}{T_{2i}}\right]\cdot\left(1-\exp\left[\frac{-TR}{T_{1i}}\right]\right). \quad (3)$$

$Si(0)$ is a function each compartment's equilibrium proton spin density (ρ_i), T_1 relaxation time (T_{1i}), T_2 relaxation time (T_{2i}), repetition time (TR), and echo time (TE).

As the diffusivity of both GM and CSF can be assumed to be isotropic, Eq. (1) can be extended to define the local CSF contamination effect on the mean diffusivity measurement.

$$\exp(-b\overline{D}(k)) = \lambda_{app-gm}(k)\cdot\exp(-b\overline{D}_{gm}(k)) + \lambda_{app-csf}(k)\cdot\exp(-b\overline{D}_{csf}(k)), \quad (4)$$

where D is the observed mean diffusivity value with CSF contamination effect in the local cortical region (k). $\overline{D}_{gm}$ and $\overline{D}_{csf}$ denote the estimated mean diffusivity value of GM and CSF. Here, $\overline{D}_{csf}$ was set to 3.0×10^{-3} m m^2/s.

Computational framework for CSF contamination effect modeling

Based on the model description above, we now describe the computational framework for CSF contamination effect modeling. The computational framework for CSF contamination effect modeling is composed of seven steps, as summarized in Fig. 1. The following subsections have same order with each step expressed in Fig. 1.

Step 1. Mean diffusivity calculation

Both DTI and FLAIR DTI were corrected for distortion and motion artifact using mutual information (Maes et al., 1997). Each directional volume was individually normalized to the non-diffusion weighted volume using affine transformation provided by Statistical Parametric Mapping (SPM2, Institute of Neurology, University College of London, UK). Then, the mean diffusivity map was calculated by in-house software programmed using MATLAB (Mathworks, Natick, MA, USA).

Step 2. Construction of tissue probability map

To estimate λ_{csf} and λ_{csf}, EPI segmentation using SPM2 was applied on individual $S(0)$ volume for constructing tissue probability map (step 2 in Fig. 1). The tissue probability value in each voxel denotes the probability of GM or CSF segment volume, and ranged between zero and one.

Steps 3 and 4. Estimation of parameters

After the calculation of λ_i based on CSF tissue probability map, the $\lambda_{app\text{-}csf}$ and $\lambda_{app\text{-}gm}$ at each voxel were calculated based on Eq. (2) (step 3 in Fig. 1). Finally, $\overline{D}_{gm}$ in each voxel was estimated based on Eq. (4) (step 4 in Fig. 1). For clearness, important symbols used to describe the method are listed with its corresponding meanings in Table 1.

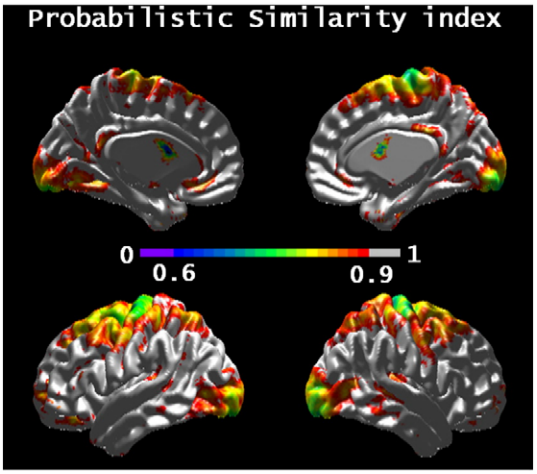

Fig. 3. Result of mean probabilistic similarity index measurement from 9 subjects. Regions above 0.9 are plotted using gray color.

Table 2
Individual result of CSF contamination modeling and its comparison result from FLAIR DTI

Subject	Mean($\overline{D}$) ($\times 10^{-4}$)	Mean($\overline{D}_{gm}$) ($\times 10^{-4}$)	Mean($\overline{D}_{flair}$) ($\times 10^{-4}$)	Mean ($\overline{D}$–$\overline{D}_{flair}$) (%)	Mean ($\overline{D}_{gm}$–$\overline{D}_{flair}$) (%)
1	7.92	6.83	6.53	23.80	6.18
2	7.84	7.51	6.46	25.37	13.14
3	8.25	7.35	6.93	21.48	9.64
4	7.12	6.32	6.17	19.02	5.81
5	7.13	6.51	6.11	21.09	7.88
6	7.27	6.54	6.15	21.29	7.21
7	9.11	7.01	7.55	25.57	14.90
8	8.29	7.50	7.09	19.09	9.58
9	8.26	7.01	7.19	27.68	11.49
10	7.74	6.78	6.67	22.54	9.32
11	7.56	6.72	6.56	24.63	8.74
12	8.01	7.12	7.02	17.52	6.53
13	7.86	7.23	7.04	15.36	5.55
14	7.54	7.21	6.54	16.35	6.23
15	8.21	7.05	6.97	23.47	10.29

Step 5. Coregistration

To accurately estimate the intracranial correspondence between structural and diffusion weighted spaces, the high resolution anatomical image and the $S(0)$ volume of both DTI and FLAIR DTI were initially skull-stripped using Oxford FSL BET (Smith, 2000) (http://www.fmrib.ox.ac.uk/analysis/research/bet). Affine and non-linear transformation parameter estimation was performed between the high resolution anatomical image and the $S(0)$ image using SPM2 (step 5 in Fig. 1). Based on the estimated transformation parameter, reconstructed cortical surface was inverse transformed to DTI space for estimating partial volume fraction and diffusion data mapping. This was to avoid error effect due to the interpolation procedure.

Step 6. Cortical surface modeling

Cortical surfaces were automatically extracted from each high resolution anatomical scan using the Constrained Laplacian-based Automated Segmentation with Proximities (CLASP) algorithm (Kim et al., 2005). CLASP reconstructs the inner cortical surface by deforming a spherical mesh onto the boundary separating the GM and WM. Deformation begins with a low-resolution polyhedral surface (320 surface points), which is deformed to fit the image data and resampled to contain more triangles (80,920 points). The outer cortical surface is expanded from the inner surface to the boundary between gray and white matter along a Laplacian map, which smoothly increases the potential surface between the gray/white and gray/CSF boundaries. During the expansion, the refined CSF fraction image is used as a constraint for accurate representation of buried sulci. Here, as the gray/CSF surface was generated from the gray/white surface, point-to-point correspondence between the two surfaces was automatically defined after final surface reconstruction.

Step 7. Surface mapping

Voxel information, including $\overline{D}$, $\overline{D}_{gm}$, $\lambda_{app\text{-}csf}$ and FLAIR mean diffusivity ($\overline{D}_{flair}$), were directly mapped to surface points using the nearest-neighbor projection method (step 7 in Fig. 1). Using the fine-surface registration technique (Lyttelton et al., 2007), each subject's surface information was mapped to an average surface template for group analysis. Finally, all the comparison and analyses were performed on the surface space.

Validation

Reliability of tissue probability estimation

As the quality of the $S(0)$ segmentation could strongly affect D_{gm} estimation, $S(0)$ segmentation results were d by estimating probabilistic similarity index (PSI) (Anbeek et al., 2004) between T1 GM segmentation map and $S(0)$ GM tissue probability map (Fig. 2a). Here, PSI was measured in each cortical surface point. Local sphere with 5 mm radius was used for measuring local PSI. PSI was defined as follow:

$$\mathrm{PSI} = \frac{2\tilde{n}\sum P_{b0gm.T1gm=1}}{\sum 1_{T1gm} + \sum P_{b0gm}}, \tag{5}$$

where $\sum P_{b0gm.T1gm=1}$ is sum over all voxel probabilities of GM tissue probability map from $S(0)$ in local region (Fig. 2b). Only counts

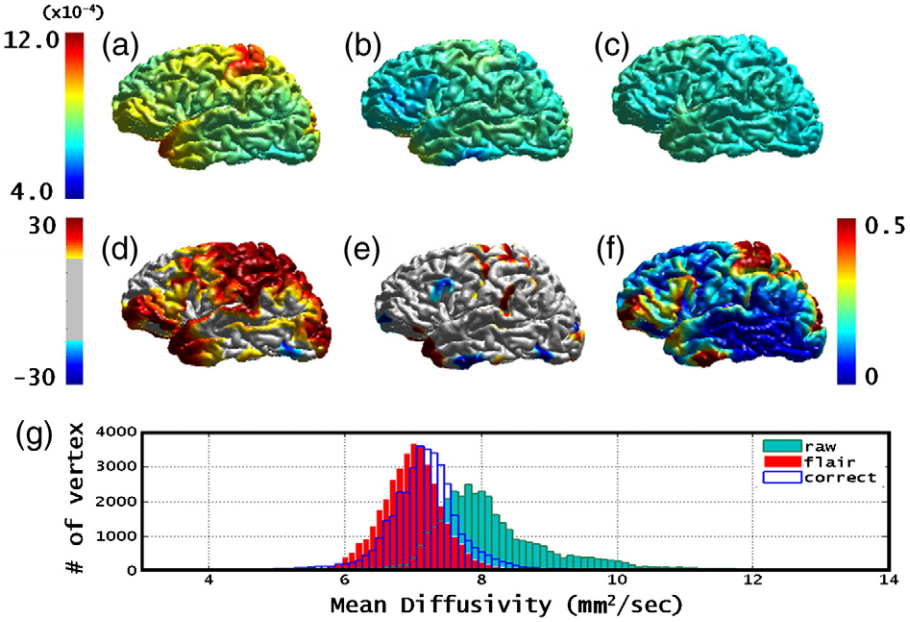

Fig. 4. Individual result of CSF contamination modeling and its comparison result from FLAIR DTI. Subject 1 in Table 2 was used to display. Mean diffusivity map ($\overline{D}$) and its corrected result ($\overline{D}_{gm}$) is in (a) and (b). (c) is the mean diffusivity map of FLAIR DTI ($\overline{D}_{flair}$). Percent differences between $\overline{D}$ and $\overline{D}_{flair}$ is in (d). Also, Percent differences between $\overline{D}_{gm}$ and $\overline{D}_{flair}$ is in (e). (f) is the estimated CSF apparent signal fraction weight (λ_{csf}). Change of the histogram due to the CSF contamination correction is displayed in (g). Note that, (a), (b), and (c) follows the color bar in left the side of (a). (d) and (e) follows the color bar in the left side of (d).

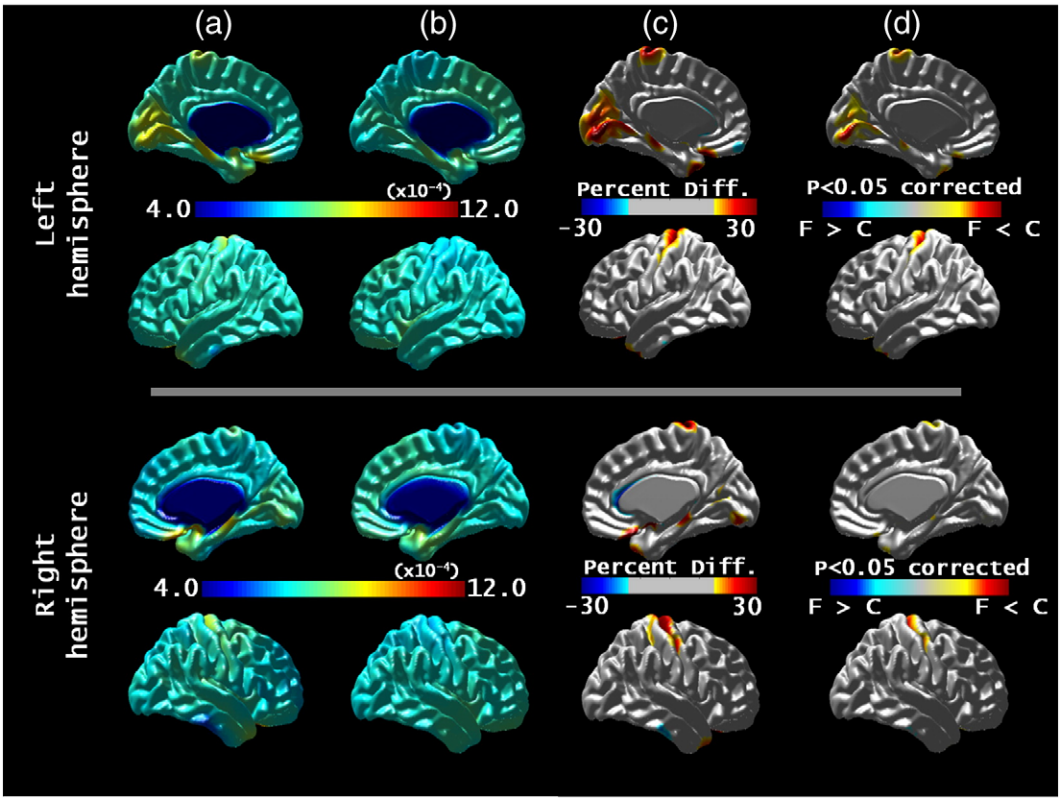

Fig. 5. Average result of CSF contamination modeling and its comparison result from FLAIR DTI. The First row is results for left hemisphere and the second is results for right hemisphere. (a) is corrected mean diffusivity map ($\overline{D}_{gm}$). (b) is the mean diffusivity map from FLAIR DTI($\overline{D}_{flair}$). (c) is difference between $\overline{D}_{gm}$ and $\overline{D}_{flair}$. Yellow-red color denotes greater $\overline{D}_{gm}$ and blue-light blue color denotes greater $\overline{D}_{flair}$. Note that values under 15% were colored in gray. (d) is the paired *t*-test result ($P<0.05$, with FDR correction). F>C has greater $\overline{D}_{flair}$ and F<C has greater $\overline{D}_{gm}$.

the probabilities in the T1 GM segment equals 1. $\sum 1_{T1gm}$ is sum over all voxels in T1 GM segment (Fig. 2c). $\sum P_{b0gm}$ is sum over all voxel probabilities over all voxel probabilities of GM tissue probability map from $S(0)$ in local region.

Comparisons with FLAIR DTI

Fifteen matched sets of conventional DTI and FLAIR DTI data were used for assessing reliability of the proposed regional modeling technique for the CSF contamination effect on GM measurement. Difference between estimated $\overline{D}_{gm}$ and $\overline{D}_{flair}$ was calculated in each subjects. Also, average difference patterns from 15 matched data were measured.

Analysis of regional CSF contamination effect

Regional pattern differences of CSF contamination effect

Regional pattern of signal bias was assessed from the comparison between $\overline{D}_{gm}$ and $\overline{D}$ of 15 subjects for testing the hypothesis on regional specificity of CSF contamination effect. Difference between estimated $\overline{D}_{gm}$ and $\overline{D}$ was measured in each subjects, and mean difference was mapped for assessing spatial patterns. Also, regional pattern of tissue compounding ratio ($\lambda_{app\text{-}csf}$) was assessed to describe localized pattern of CSF contamination effect.

Relationships with GM morphology

Both cortical thickness and local curvature of GM were used to interpret the local CSF contamination effect in terms of the morphological characteristics of GM. As the gray/CSF surface was derived from the gray/white surface in our surface modeling technique, local point-to-point correspondences between two surfaces were automatically defined after final surface reconstruction. Thus, cortical thickness was measured automatically (Lerch and Evans, 2005) and then used to assess relationship between CSF contamination effect and cortical thickness. Local curvature was calculated automatically on GM/CSF surface based on mean curvature calculation scheme (Meyer et al., 2002).

Results

Validation

Reliability of tissue probability estimation

The quality of the $S(0)$ segmentation was validated based on local PSI measurement as shown in Fig. 3. Most of region showed the local PSI above 0.9, which means 90% similarity with high resolution T1 segmentation result. Maximum error of $S(0)$ segmentation was observed in the precentral gyrus and the primary visual area. The somatosensory association cortex and the supplementary motor area displayed local PSI values in the range of 0.75 to 0.9. Also, small clusters with local PSI values around 0.8 were found in the inferior prefrontal region, the mid temporal lobe, the ventral posterior cingulated gyrus.

Comparisons with FLAIR DTI

The CSF contamination modeling framework proposed in this study was directly compared with matching FLAIR DTI data. Individual CSF contamination modeling effect is shown in Table 2. Mean differences between DTI and FLAIR DTI was significantly reduced after the elimination of CSF contamination effect. Also, spatial pattern differences are shown in Fig. 4. GM mean diffusivity without CSF contamination correction of individual subject (Fig. 4a) showed above 50% signal increase in superior part of the brain in comparison to FLAIR DTI (Fig. 4c). Also, the prefrontal lobe, the occipital lobe and the temporal pole region displayed significant increase of mean diffusivity (Fig. 4d). Those significant biases were reduced after the CSF contamination modeling (Figs. 4b,e). Estimated apparent CSF volume

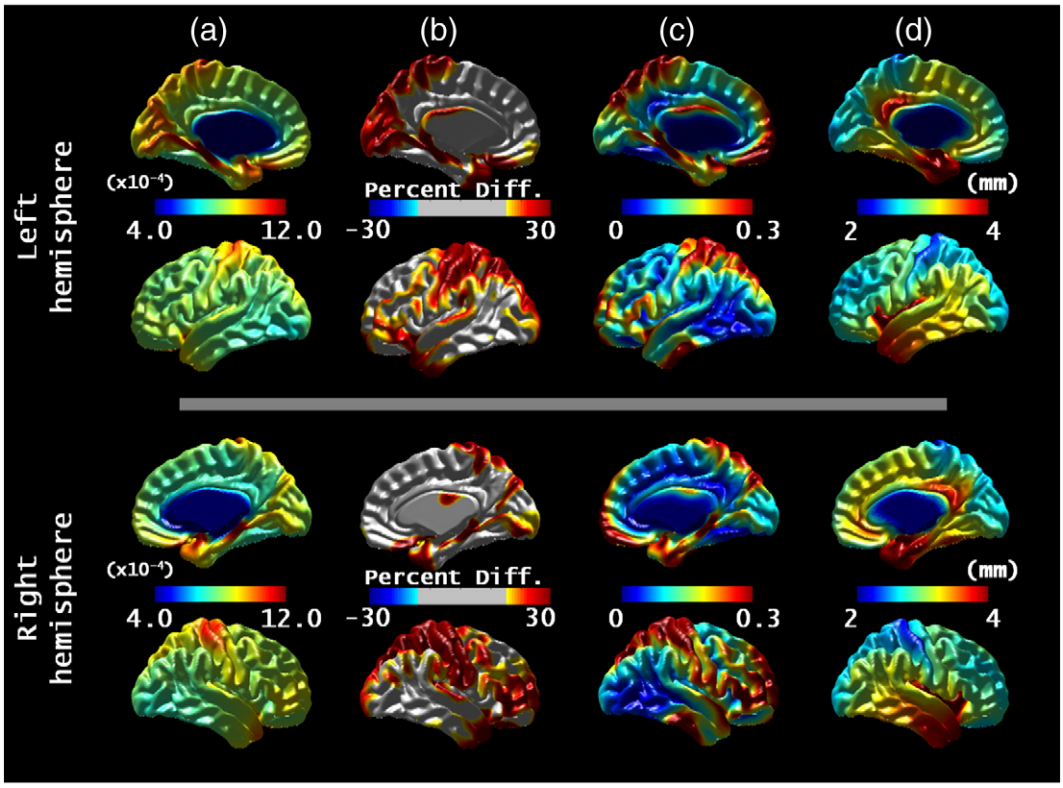

Fig. 6. Average properties of relative CSF contamination effect on GM mean diffusion measurements from 15 subjects. The First row is results for left hemisphere and the second is results for right hemisphere. (a) is the mean diffusivity map ($\overline{D}$).(b) is difference between $\overline{D}$ and $\overline{D}_{gm}$. Yellow-red color denotes greater $\overline{D}$ and blue-light blue color denotes greater $\overline{D}_{gm}$. Note that values under 15% were colored in gray. (c) is the estimated CSF apparent signal fraction weight (λ_{csf}). (d) is the average cortical thickness.

fraction ($\lambda_{app\text{-}csf}$) is shown in Fig. 4f. Histogram of GM mean diffusivity showed higher similarity with FLAIR DTI after the elimination of CSF contamination (Fig. 4g).

Group average pattern after modeling of CSF contamination for 15 subjects was compared to their matching FLAIR DTI data as shown in Fig. 5. Estimated $\overline{D}_{gm}$ (Fig. 5a) resulted in similar ranges of $\overline{D}_{flair}$ (Fig. 5b) except for the superior part of pre and post central region, the parahippocampal gyrus, anterior part of the entorhinal cortex, and medial part of the visual cortex (Fig. 5c). However, paired *t*-test ($P<0.05$ with FDR correction) between DTI and FLAIR DTI showed significant differences in superior part of the central sulcus and medial part of the visual cortex (Fig. 5d).

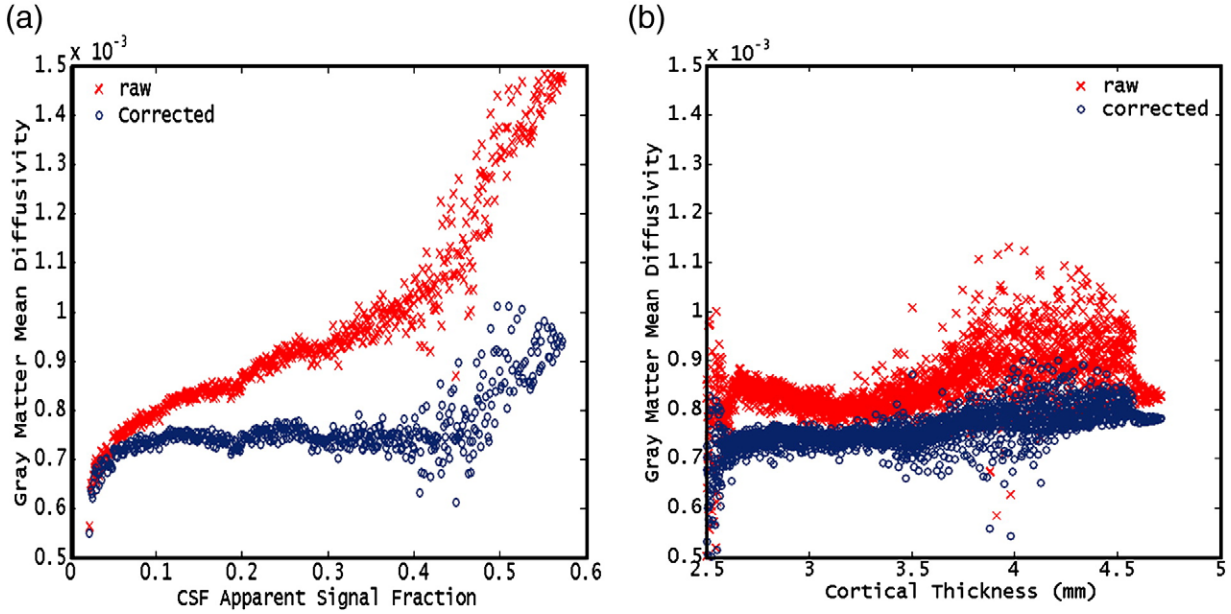

Fig. 7. Relationship between $\lambda_{app\text{-}csf}$ and $\overline{D}$ is in (a). Relationship between $\overline{D}$ and cortical thickness measurement is shown in (b). The red color plot denotes $\overline{D}$ and blue color denotes $\overline{D}_{gm}$.

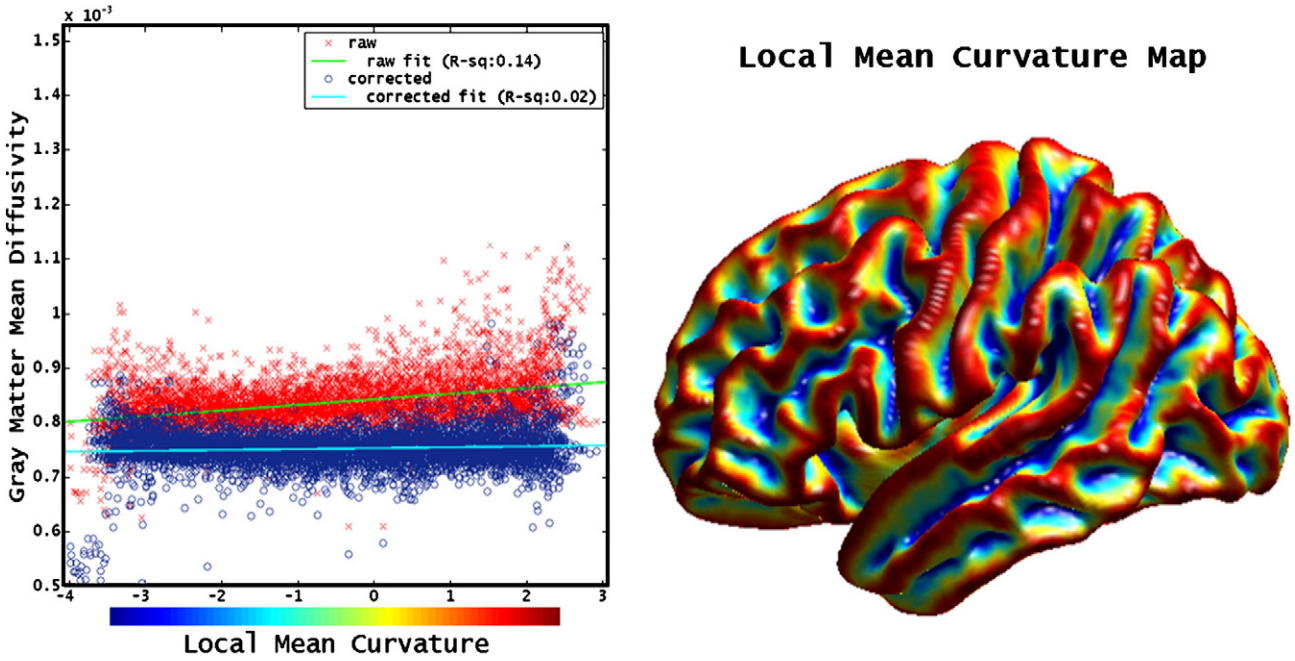

Fig. 8. Relationship between local mean curvature and CSF contamination effect is shown in left side. The red color plot denotes $\overline{D}$ and blue color denotes $\overline{D}_{gm}$. Local mean curvature map is shown in right side. The corresponding color bar is displayed in the lower part of the graph.

Analysis of regional CSF contamination effect

Regional pattern differences of CSF contamination effect

Surface mapping of D from the 15 subjects is displayed in Fig. 6a. The maximum $\overline{D}$ values are shown in superior part of the pre-/postcentral gyri, the parahippocampal gyrus, and medial part of the visual cortex. The difference between $\overline{D}_{gm}$ and $\overline{D}$ (Fig. 6b) provides clear figure of estimated signal bias. Over 50% signal increases were observed in superior part of the pre-/postcentral gyri, the superior parietal lobe, medial part of the visual cortex and the parahippocampal gyrus. Over 30% signal biases were observed in lateral part of the prefrontal region and the temporal pole. Also, over 15% signal increases were shown in the mid and the inferior frontal gyri, the superior temporal gyrus. The regional estimation of $\lambda_{app\text{-}csf}$ is shown in Fig. 6c. Here, $\lambda_{app\text{-}csf}$ maps exhibit a similar spatial pattern of signal bias as seen in Fig. 6b. Significant mutual relationship between $\lambda_{app\text{-}csf}$ and D is shown in Fig. 7a.

Relationships with GM morphology

Relationship between local cortical thickness (Fig. 6d) and CSF contamination effect (Fig. 6b) is shown in Fig. 7b. Cortical thickness ranging between 2.5 to 3.5 mm displayed linear decrease pattern and cortical thickness above 3.5 mm showed large variances. After the elimination of CSF contamination, mean diffusivity of GM showed slight increase with cortical thickness. Also, the variance was reduced. Also, relationship between local cortical thickness and CSF contamination effect is shown in the left side of Fig. 8. The region with negative curvature which shown in sulcal banks (right side of Fig. 8) had minimum signal bias. Moreover, signal bias was increased when the curvature increased.

Discussion

In this study, relationships between the GM mean diffusivity measurement and the CSF contamination effect were quantitatively assessed within a regional modeling framework. From Latour and Warach (2002), it could have been expected that CSF averaging with GM in a voxel would provide significant mean diffusivity signal increase (almost twice as much as volume fraction ratio of CSF itself). However, due to the coarse resolution of typical diffusion weighted imaging and the resulting limitation on partial volume fraction estimation, it was not possible to use the partial volume model on more realistic sets of data. In this study, high resolution DTI with 1.88×1.88×2.00 mm size voxel was obtained, and the degree of regional CSF contamination effects on GM mean diffusivity measurement were properly estimated from the two compartment model. Moreover, relationship between CSF contamination effect and local macroscopic morphology was assessed without difficulty from cortical surface modeling methods.

Validation

Reliability of tissue probability estimation

Related parameters, such as $\lambda_{app\text{-}gm}$ and $\lambda_{app\text{-}csf}$, were efficiently estimated from segmenting $S(0)$ volume using EPI segmentation algorithm. Quality of $S(0)$ segmentation using the local PSI index showed efficiency of the tissue probability estimation. This may indicate that SPM-based estimation of tissue probability can be a proper method for estimating critical parameters on CSF contamination modeling. However, the GM region with thin cortical thickness (below 2.5 mm), such as precentral gyrus, the primary visual area, and somatosensory cortex, showed poor segmentation result in spite of relatively high resolution of DTI data. Such segmentation error may critically increase in coarse resolution dataset. Thus, we could conclude that the maximum 2 mm voxel resolution is critical to analyze the GM microstructure.

Comparisons with FLAIR DTI

Overall consistency between estimated GM mean diffusivity and the FLAIR DTI comparison results indicate that proposed modeling technique based on two compartment model will be adequate for handling the critical issues on GM mean diffusivity measurement. Moreover, significant change in cumulative distribution after the elimination of estimated CSF contamination effect (Fig. 4g) suggests that our data strongly agrees with other studies (Bhagat and Beaulieu, 2004; Liu et al., 2006). However, from Figs. 3 and 5c, it is clear that inconsistency between $\overline{D}_{gm}$ and $\overline{D}_{flair}$ can be explained by poor segmentation result shown in precentral gyrus and the primary visual

area. Thus, those regions with inconsistencies need to be carefully considered for analyze CSF contamination effect.

Analysis of regional CSF contamination effect

Regional pattern differences of CSF contamination effect

Our data (Fig. 6) showed the regional specificity of CSF contamination effect due to local morphological differences. More specifically, the local CSF volume fraction varies with local morphology. The sub-arachnoid space, which contains the extracortical CSF, is known to have a minimal volume near the top of gyral region, and, in the sulcal region, it is filled with sponge-like sub-arachnoid trabecular tissue that extends from the arachnoid matter and merges into the pia. Also, the superior and ambient cisterns show the sub-arachnoidal space to be maximal. These properties can be confirmed from local CSF volume fraction map in Fig. 6c. Thus, it is clear that estimation of CSF volume fraction in each GM voxel is most critical factor for measuring GM mean diffusivity (Fig. 7a).

Relationships with GM morphology

Our results suggest that macroscopic morphology, such as the geometrical complexity and the thickness of GM, strongly contributes to produce region specific difference of heterogeneous tissue averaging. Considering Fig. 7b, the regions that had significantly higher D ranges were significantly thinner (2–2.5 mm) than other regions. Also, the regions that had significantly lower D ranges were significantly thicker (above 3.5 mm) than other regions. The regions with relatively thin GM, such as superior part of the pre-/postcentral gyri and the superior parietal lobe showed higher possibility of CSF compartment than the region with thick GM structure. This means that thick cortical structure may decrease the possibility of CSF contamination. Oppositely, thin GM structure such as the visual cortex showed relatively lower possibility of CSF compartment. Those differences may due to the local morphology of sub-arachnoid space. Thus, GM region adjacent to relatively small sub-arachnoidal space, such as visual cortex, may have different amount of CSF contamination.

CSF contamination may also vary with sulcal geometry, depth, and width in the sulcal region within the gyrus. In Fig. 8, highly curved structure in gyral region may have high possibility of CSF contamination. Oppositely, highly curved structures in deep sulcal region have low possibility of CSF contamination. Also, sulcal wall may have less probability of CSF contamination in comparison to top of gyral region. These properties can be changed due to the sulcal widening process, which is important factor for analyzing various diseases.

As we showed in Fig. 6, above 20% CSF contamination on local region induce significant signal bias on GM mean diffusion measurement. Thus, the regional differences in GM mean diffusivity without CSF contamination correction can be interpreted to local GM structural changes rather than intrinsic GM diffusivity. Moreover, the effect of $\lambda_{app\text{-}csf}$ on group statistical analysis needs to be emphasized for important covariant on GM mean diffusivity analysis.

Considerations for clinical analysis

Relationship between GM mean diffusivity measurement and various clinical factors were reported in many studies (Bozzali et al., 2002; Cercignani et al., 2001; Kumar et al., 2006; Liu et al., 2006; Ray et al., 2006; Rovaris et al., 2002, 2005, 2006). Possible interpretation for those clinical related characteristics of GM mean diffusivity can be divided into two factors: tissue loss and microstructural status of the remaining tissue. As we mentioned in the previous section, the former factor may have higher probabilities to provide direct cause of heterogeneity. Local shrinkage of volume or sulcal widening can be followed by tissue loss effect, and such morphological change may provide more possibilities of CSF contamination. Therefore, multivariate analysis including both microscopic and macroscopic GM structure is critical for explicit analysis. Although some reports applied it to GM mean diffusivity analysis and successfully describe more clear interpretations for clinical related GM mean diffusivity changes (Benedetti et al., 2006; Rovaris et al., 2005), the scope of analysis was restrict to whole volume level. For assessing localized changes in relation to clinical symptoms, the scope of analysis needs to be focused on specific region.

Our proposed modeling framework has three advantages over previous approaches (Alexander et al., 2001; Liu et al., 2006). Firstly, localized analysis of GM diffusion measurement with consideration of possible bias is made possible. To our knowledge, there is no other suitable localized analysis method providing overall spatial pattern. Although Liu et al. (Liu et al., 2006) proposed a fully automatic ROI-based analysis for cortical GM mean diffusivity, our technique is capable of further, more subtle analysis. Secondly, group analysis may have more success using the surface-based technique: avoiding the reslicing effect during volume registration that can induce the additional bias; providing consistent group registration for analysis (Lyttelton et al., 2007). Finally, it may be possible to extend analysis to other structural analyses such as cortical thickness measurement or functional analysis. Therefore, our proposed framework for GM mean diffusivity measurement under estimation of CSF contamination effect may provide one efficient way for various clinical analyses. Clinical application of our proposed method will need to be addressed in our following study.

Conclusion

We proposed a framework on modeling and analysis of the CSF contamination effect on GM mean diffusivity measurements. Two-compartment model with local tissue proportion estimation was successfully applied to correct and interpret possible measurement biases which may lead unclear interpretation of clinical GM mean diffusivity analysis. Our result indicates that the local peripheral morphology is critical to understand intrinsic meaning of locally different GM mean diffusion property. Thus, we recommend considering multivariate analysis which includes both GM mean diffusivity and estimated CSF contamination for group-specific studies.

Acknowledgments

This work was supported by the Korea Science and Engineering Foundation (KOSEF) NRL program grant funded by the Korea government (MEST) (R0A-2007-000-20068-0).

References

Alexander, A.L., Hasan, K.M., Lazar, M., Tsuruda, J.S., Parker, D.L., 2001. Analysis of partial volume effects in diffusion-tensor MRI. Magn. Reson. Med. 45, 770–780.
Anbeek, P., Vincken, K.L., van Osch, M.J., Bisschops, R.H., van der Grond, J., 2004. Probabilistic segmentation of white matter lesions in MR imaging. Neuroimage 21, 1037–1044.
Basser, P.J., 1995. Inferring microstructural features and the physiological state of tissues from diffusion-weighted images. NMR. Biomed. 8, 333–344.
Beaulieu, C., 2002. The basis of anisotropic water diffusion in the nervous system—a technical review. NMR. Biomed. 15, 435–455.
Benedetti, B., Charil, A., Rovaris, M., Judica, E., Valsasina, P., Sormani, M.P., Filippi, M., 2006. Influence of aging on brain gray and white matter changes assessed by conventional, MT, and DT MRI. Neurology 66, 535–539.
Bhagat, Y.A., Beaulieu, C., 2004. Diffusion anisotropy in subcortical white matter and cortical gray matter: changes with aging and the role of CSF-suppression. J. Magn. Reson. Imaging 20, 216–227.
Bozzali, M., Cercignani, M., Sormani, M.P., Comi, G., Filippi, M., 2002. Quantification of brain gray matter damage in different MS phenotypes by use of diffusion tensor MR imaging. AJNR Am. J. Neuroradiol. 23, 985–988.
Camara, E., Bodammer, N., Rodriguez-Fornells, A., Tempelmann, C., 2007. Age-related water diffusion changes in human brain: a voxel-based approach. Neuroimage 34, 1588–1599.
Cercignani, M., Bozzali, M., Iannucci, G., Comi, G., Filippi, M., 2001. Magnetisation transfer ratio and mean diffusivity of normal appearing white and grey matter from patients with multiple sclerosis. J. Neurol. Neurosurg. Psychiatry 70, 311–317.
Dale, A.M., Fischl, B., Sereno, M.I., 1999. Cortical surface-based analysis. I. Segmentation and surface reconstruction. Neuroimage 9, 179–194.

Falconer, J.C., Narayana, P.A., 1997. Cerebrospinal fluid-suppressed high-resolution diffusion imaging of human brain. Magn. Reson. Med. 37, 119–123.
Fischl, B., Sereno, M.I., Dale, A.M., 1999. Cortical surface-based analysis. II: inflation, flattening, and a surface-based coordinate system. Neuroimage 9, 195–207.
Helenius, J., Soinne, L., Perkio, J., Salonen, O., Kangasmaki, A., Kaste, M., Carano, R.A., Aronen, H.J., Tatlisumak, T., 2002. Diffusion-weighted MR imaging in normal human brains in various age groups. AJNR. Am. J. Neuroradiol. 23, 194–199.
Horsfield, M.A., Jones, D.K., 2002. Applications of diffusion-weighted and diffusion tensor MRI to white matter diseases—a review. NMR. Biomed. 15, 570–577.
Jo, H.J., Lee, J.M., Kim, J.H., Shin, Y.W., Kim, I.Y., Kwon, J.S., Kim, S.I., 2007. Spatial accuracy of fMRI activation influenced by volume- and surface-based spatial smoothing techniques. Neuroimage 34, 550–564.
Kim, J.S., Singh, V., Lee, J.K., Lerch, J., Ad-Dab'bagh, Y., MacDonald, D., Lee, J.M., Kim, S.I., Evans, A.C., 2005. Automated 3-D extraction and evaluation of the inner and outer cortical surfaces using a Laplacian map and partial volume effect classification. Neuroimage 27, 210–221.
Kubicki, M., Westin, C.F., Maier, S.E., Mamata, H., Frumin, M., Ersner-Hershfield, H., Kikinis, R., Jolesz, F.A., McCarley, R., Shenton, M.E., 2002. Diffusion tensor imaging and its application to neuropsychiatric disorders. Harv. Rev. Psychiatry 10, 324–336.
Kumar, R., Macey, P.M., Woo, M.A., Alger, J.R., Harper, R.M., 2006. Elevated mean diffusivity in widespread brain regions in congenital central hypoventilation syndrome. J. Magn. Reson. Imaging 24, 1252–1258.
Kwong, K.K., McKinstry, R.C., Chien, D., Crawley, A.P., Pearlman, J.D., Rosen, B.R., 1991. CSF-suppressed quantitative single-shot diffusion imaging. Magn. Reson. Med. 21, 157–163.
Latour, L.L., Warach, S., 2002. Cerebral spinal fluid contamination of the measurement of the apparent diffusion coefficient of water in acute stroke. Magn. Reson. Med. 48, 478–486.
Le Bihan, D., 1995. Molecular diffusion, tissue microdynamics and microstructure. NMR. Biomed. 8, 375–386.
Lee, J.K., Lee, J.M., Kim, J.S., Kim, I.Y., Evans, A.C., Kim, S.I., 2006. A novel quantitative cross-validation of different cortical surface reconstruction algorithms using MRI phantom. Neuroimage. 31, 572–584.
Lerch, J.P., Evans, A.C., 2005. Cortical thickness analysis examined through power analysis and a population simulation. Neuroimage 24, 163–173.
Liu, T., Young, G., Huang, L., Chen, N.K., Wong, S.T., 2006. 76-space analysis of grey matter diffusivity: methods and applications. Neuroimage 31, 51–65.
Lyttelton, O., Boucher, M., Robbins, S., Evans, A., 2007. An unbiased iterative group registration template for cortical surface analysis. Neuroimage 34, 1535–1544.
Maes, F., Collignon, A., Vandermeulen, D., Marchal, G., Suetens, P., 1997. Multimodality image registration by maximization of mutual information. IEEE. Trans. Med. Imaging 16, 187–198.
Meyer, M., Desbrun, M., Schroder, P., Barr, A.H., 2002. Discrete differential-geometry operators for triangulated 2-manifolds. Vis. Math 35–58.
Moseley, M., 2002. Diffusion tensor imaging and aging—a review. NMR. Biomed. 15, 553–560.
Neil, J., Miller, J., Mukherjee, P., Huppi, P.S., 2002. Diffusion tensor imaging of normal and injured developing human brain—a technical review. NMR. Biomed. 15, 543–552.
Niendorf, T., Dijkhuizen, R.M., Norris, D.G., van Lookeren Campagne, M., Nicolay, K., 1996. Biexponential diffusion attenuation in various states of brain tissue: implications for diffusion-weighted imaging. Magn. Reson. Med. 36, 847–857.
Park, H.J., Lee, J.D., Chun, J.W., Seok, J.H., Yun, M., Oh, M.K., Kim, J.J., 2006. Cortical surface-based analysis of 18F-FDG PET: measured metabolic abnormalities in schizophrenia are affected by cortical structural abnormalities. Neuroimage 31, 1434–1444.
Ray, K.M., Wang, H., Chu, Y., Chen, Y.F., Bert, A., Hasso, A.N., Su, M.Y., 2006. Mild cognitive impairment: apparent diffusion coefficient in regional gray matter and white matter structures. Radiology 241, 197–205.
Rovaris, M., Bozzali, M., Iannucci, G., Ghezzi, A., Caputo, D., Montanari, E., Bertolotto, A., Bergamaschi, R., Capra, R., Mancardi, G.L., Martinelli, V., Comi, G., Filippi, M., 2002. Assessment of normal-appearing white and gray matter in patients with primary progressive multiple sclerosis: a diffusion-tensor magnetic resonance imaging study. Arch. Neurol. 59, 1406–1412.
Rovaris, M., Gallo, A., Valsasina, P., Benedetti, B., Caputo, D., Ghezzi, A., Montanari, E., Sormani, M.P., Bertolotto, A., Mancardi, G., Bergamaschi, R., Martinelli, V., Comi, G., Filippi, M., 2005. Short-term accrual of gray matter pathology in patients with progressive multiple sclerosis: an in vivo study using diffusion tensor MRI. Neuroimage 24, 1139–1146.
Rovaris, M., Judica, E., Gallo, A., Benedetti, B., Sormani, M.P., Caputo, D., Ghezzi, A., Montanari, E., Bertolotto, A., Mancardi, G., Bergamaschi, R., Martinelli, V., Comi, G., Filippi, M., 2006. Grey matter damage predicts the evolution of primary progressive multiple sclerosis at 5 years. Brain 129, 2628–2634.
Smith, S.M., 2000. BET: Brain Extraction Tool. FMRIB Techn. Rep. TR00SMS2B, 1–25.
Zilles, K., Armstrong, E., Schleicher, A., Kretschmann, H.J., 1988. The human pattern of gyrification in the cerebral cortex. Anat Embryol (Berl) 179, 173–179.